

Mechanisms of Interannual Variations of the Meridional Overturning Circulation of the North Atlantic Ocean

CÉCILE CABANES, TONG LEE, AND LEE-LUENG FU

Jet Propulsion Laboratory, California Institute of Technology, Pasadena, California

(Manuscript received 15 November 2006, in final form 30 April 2007)

ABSTRACT

The authors investigate the nature of the interannual variability of the meridional overturning circulation (MOC) of the North Atlantic Ocean using an Estimating the Circulation and Climate of the Ocean (ECCO) assimilation product for the period of 1993–2003. The time series of the first empirical orthogonal function of the MOC is found to be correlated with the North Atlantic Oscillation (NAO) index, while the associated circulation anomalies correspond to cells extending over the full ocean depth. Model sensitivity experiments suggest that the wind is responsible for most of this interannual variability, at least south of 40°N. A dynamical decomposition of the meridional streamfunction allows a further look into the mechanisms. In particular, the contributions associated with 1) the Ekman flow and its depth-independent compensation, 2) the vertical shear flow, and 3) the barotropic gyre flowing over zonally varying topography are examined. Ekman processes are found to dominate the shorter time scales (1.5–3 yr), while for longer time scales (3–10 yr) the MOC variations associated with vertical shear flow are of greater importance. The latter is primarily caused by heaving of the pycnocline in the western subtropics associated with the stronger wind forcing. Finally, how these changes in the MOC affect the meridional heat transport (MHT) is examined. It is found that overall, Ekman processes explain a larger part of interannual variability (3–10 yr) for MHT (57%) than for the MOC (33%).

1. Introduction

The meridional overturning circulation (MOC) of the North Atlantic Ocean is the main carrier of the meridional heat transport (MHT) of this ocean and therefore has potentially important climatic significance. Seasonal variations of the MOC and MHT in the North Atlantic Ocean have been studied extensively (e.g., Häkkinen 1999; Jayne and Marotzke 2001; Hall et al. 2004; Köhl 2005). The primary conclusion is that the variations of zonal wind stress and the resultant meridional Ekman flow anomalies are responsible for most of the seasonal variability in MHT, as achieved by Ekman flow advecting warm surface water in one direction and subsurface compensating flow advecting colder subsurface temperature in the opposite direction. On decadal and longer time scales, previous studies suggest the importance of buoyancy forcing and the involvement of the deep geostrophic flow associated with the MOC

variations (e.g., Häkkinen 2001; Dong and Sutton 2001; Bryden et al. 2005).

Interannual variations of MOC and MHT are not well documented. Dong and Sutton (2001) analyzed the output from a coupled ocean–atmosphere model and found that the first EOF of the MOC and MHT, dominated by interannual variability between the equator and 30°N, is largely associated with wind stress forcing and accounts for about half of the variance of the MHT. Interannual variability north of 30°N and south of the equator are not represented by this mode. The structure of the MOC associated with this mode (their Fig. 2e) is characterized by surface Ekman flow compensated by subsurface return flow in the northern tropical band. In the subtropics (e.g., 30°N), however, the MOC structure has a maximum around the depth of 1000 m. This feature, not discussed in their paper, suggests that Ekman flow and subsurface compensation cannot explain the interannual variations of MOC in the subtropics. In other words, zonal wind stress is not the dominant forcing for MOC variability there. Hall et al. (2004) analyzed the output of a forced ocean model for the period of 1980 to 2000 and found that Ekman re-

Corresponding author address: Cécile Cabanes, LPO, Ifremer, Centre de Brest, BP 70, 29280 Plouzané, France.
E-mail: cecile.cabanes@ifremer.fr

sponse to wind stress variations accounts for a significant portion of interannual variability of heat transport across a nonzonal section that lies along the path of the Gulf Stream extension (i.e., more or less under the mid-latitude westerly wind band). The nature of interannual variations of the Atlantic MOC and its forcing mechanisms require further study.

The potential role of forcings other than zonal wind stress has been suggested by other studies. For example, Häkkinen (2001) use a forced ocean model and sea level observations in the 1990s to study the qualitative relation between sea level variability and MOC. She found that sea level can be used as a proxy indicator for the interannual variability of MOC. In particular, the large sea surface height (SSH) change near the Gulf Stream around 1995–96 corresponds to a weakening of the MOC. Such SSH variability suggests the possible role of other forcings (e.g., wind stress curl or Ekman pumping, or surface buoyancy forcing) in addition to wind stress itself. Therefore, the relative contribution by different forcings on interannual variations of the MOC in the Atlantic Ocean needs further investigation. The nature of the interannual variability of the MOC also needs to be analyzed explicitly. While some studies suggest that the variations of Ekman flow and compensating return flow account for much of the MHT variability, there have been suggestions that the change of a horizontal gyre in the presence of zonally nonuniform topography also contributes to the variations of the MOC (Koltermann et al. 1999; Häkkinen 2001). Understanding the nature of the MOC interannual variations and its forcing mechanisms can help to better interpret the nature of the variability observed in situ systems designed to monitor the MOC.

This study intends to fill some of the aforementioned gaps in our understanding about the interannual variability of the Atlantic MOC. The specific objectives are

- 1) to investigate the latitudinal and vertical structure of the dominant interannual variability of the MOC;
- 2) to examine the forcing mechanism of the MOC variability identified in the first objective, that is, the relative contribution of wind and buoyancy forcings;
- 3) to study the mechanism through which the dominant forcing drives the dominant pattern of MOC as identified in 1) (e.g., How important is the effect of zonal wind stress that drives an “Ekman” cell? Can wind stress curl cause density gradient at depth to drive a MOC change?).

We address these science questions by analyzing an ocean analysis product and forcing sensitivity experiments. The paper is organized as follows: In section 2, we describe the ocean analysis product and the model

sensitivity experiments used to decipher the effects of different forcings. In section 3, we present the results of the analysis of dominant forcing and perform a dynamical decomposition of the MOC to isolate processes that drive the MOC variability. In section 4, we examine the consequences of the MOC on the meridional heat transport, and in section 5 summarize the finding.

2. ECCO analysis product and forcing sensitivity experiments

The analysis fields (of velocity, sea level, temperature, and salinity) used for this investigation are obtained from a data assimilation product of Estimating the Circulation and Climate of the Ocean (ECCO; <http://www.ecco-group.org>). The underlying model is a parallel version of the primitive equation Massachusetts Institute of Technology (MIT) Ocean GCM (Marshall et al. 1997). The spatial domain is nearly global (80°S–80°N). Horizontal grid spacing is 1° globally except within 20° of the equator where the meridional resolution gradually reduced to 0.3° within 10° of the equator. There are 46 vertical levels with a 10-m thickness in the upper 150 m. The model employs two advanced mixing schemes: the *K*-profile parameterization vertical mixing (Large et al. 1994) and the Gent–McWilliams isopycnal mixing (Gent and McWilliams 1990). The forcing fluxes are those from the National Centers for Environmental Prediction (NCEP) reanalysis products (12-hourly wind stress, daily heat and freshwater air–sea fluxes) with the time means replaced by those of the Comprehensive Ocean–Atmosphere Data Set fluxes (da Silva et al. 1994). Additional description of the model, the spinup, and comparison with various observational data are provided by Lee et al. (2002).

Following the spinup, a real-time integration is performed using forcing from 1980 to 1992. From 1993 to 2003, an approximate Kalman filter and smoother (Fukumori 2002) are used to assimilate anomalies of sea level and subsurface temperature obtained from the Ocean Topography Experiment (TOPEX)/Poseidon and *Jason-1* altimeters and the Global Telecommunication System (GTS) (D. Behringer 2002, personal communication), respectively. A prototype of this system was described by Fukumori et al. (1999).

The assimilation procedure corrects the prior NCEP wind forcing during an inversion by the smoother (Fukumori 2006). The modified wind forcing, referred to as τ thereafter, is then used to force the model for the period of 1993 to 2003. In addition to the imposed NCEP heat fluxes, the model sea surface temperature is relaxed to NCEP’s SST reanalysis with a time scale of

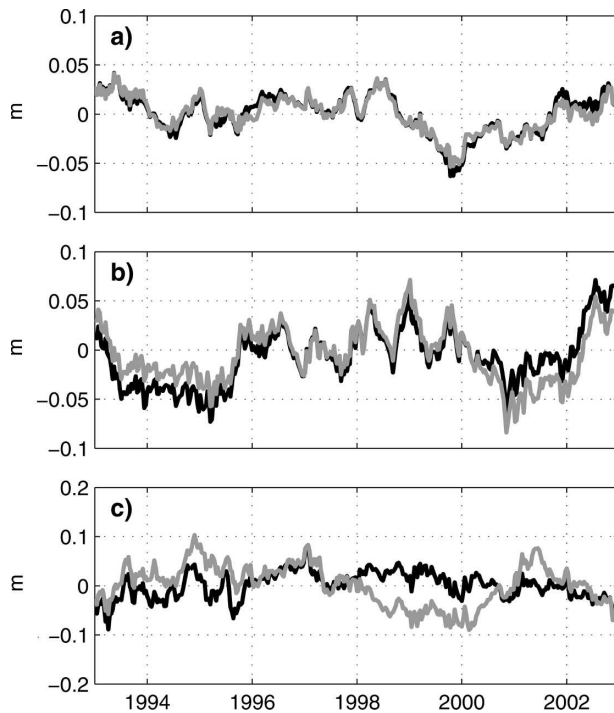


FIG. 1. Interannual sea level variations (m) in the Atlantic from REF (black) and WIND+BUOY+CLIM (gray) at (a) 14.8°N, 34.5°W; (b) 28°N, 72.5°W; and (c) 58°N, 44.5°W.

1–2 months using the formulation of Barnier et al. (1995). Similarly, the sea surface salinity (SSS) is relaxed to the Levitus 98 climatological mean salinity (Boyer and Levitus 1997). The relaxation term is therefore equivalent to an additional buoyancy flux, Q_r . The solution for this forced run is referred to as the Kalman filter/smoothing analysis. This analysis product has been used previously to study the midlatitude and tropical Pacific Ocean by Kim et al. (2004) and Kim et al. (2007).

One of the objectives of this study is to examine the relative effect of interannual wind and buoyancy forcings. For that purpose, the modified wind stress, τ , and the effective buoyancy flux, $Q_{\text{tot}} = Q_{\text{ncep}} + Q_r$, were used to force the model, without assimilation or relaxation to SST and SSS. A detailed explanation and justification of our procedure are given in the appendix. The results obtained are referred to as the REF experiment output and are very close to the original Kalman filter/smoothing analysis. We then perform sensitivity experiments with either the interannual wind or the interannual buoyancy forcing replaced by the corresponding perpetual seasonal forcing obtained from the 1993–2003 averages. The experiment denoted as CLIM uses perpetual seasonal wind and buoyancy forcings. Although there is no interannual variation in the forc-

ings, the model state of this run will exhibit interannual changes. This is because the initial state, obtained from a model integration using forcing prior to 1993, is usually not in equilibrium with the seasonal forcing computed from the 1993–2003 averages. The outputs of two other experiments denoted as WIND and BUOY contain the effect of the interannual wind forcing and the interannual buoyancy forcing for the 1993–2003 period, respectively (see the appendix).

If all processes are linear, WIND + BUOY + CLIM would be equivalent to REF. As an example to show how such forcing sensitivity experiments can isolate the effects of the initial state and different forcings, we present the sea level of REF and that computed from WIND + BUOY + CLIM for different locations: the tropical, subtropical, and midlatitude Atlantic (Fig. 1a–c). In the tropics and subtropics, WIND + BUOY + CLIM reproduces REF reasonably well because the processes are relatively linear. At high latitude where wintertime convection (a highly nonlinear process) is involved, there are relatively large differences between the interannual variability simulated by REF and that reconstructed from WIND + BUOY + CLIM.

3. Interannual variability of meridional overturning: Forcings and mechanisms

In this section we examine the mechanisms and dynamics of the interannual changes in the meridional overturning circulation. After describing the temporal and spatial structure of the low-frequency variations (periods longer than 1.5 yr) of the MOC, we investigate the role of each forcing (buoyancy and wind) using sensitivity experiments (section 3a). We then explore the dynamics that links the MOC variability to the forcing (sections 3b and 3c).

The meridional overturning streamfunction is calculated from the meridional velocity $v(x, y, z, t)$ as

$$\psi(y, z, t) = \int_{-z}^0 \int_{x_{\text{east}}(y,z)}^{x_{\text{west}}(y,z)} v(x, y, z, t) dx dz. \quad (1)$$

The time-mean meridional overturning streamfunction in the North Atlantic from REF experiment is shown in Fig. 2a. The Atlantic deep cell associated with northern deep water formation is well represented, with a maximum reaching 20 Sv ($\text{Sv} \equiv 10^6 \text{ m}^3 \text{ s}^{-1}$) around 45°N and 1000-m depth. The interannual variations of MOC over 1993–2003 are computed by low-pass filtering and detrending.

To better characterize this variability we computed the standard deviation for the 1.5–3-yr bandpass-filtered (Fig. 2b) and for the 3-yr low-pass-filtered time

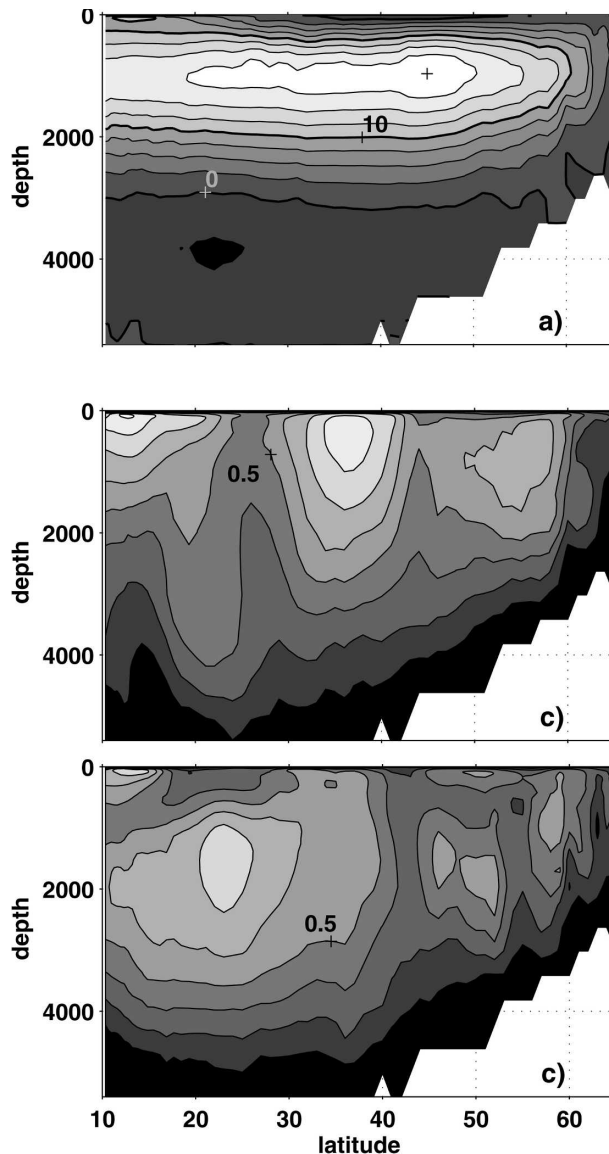


FIG. 2. Meridional overturning circulation of the North Atlantic Ocean from the REF experiment: (a) time mean (Sv) for 1993–2003, contours intervals 2.5 Sv. Standard deviation (Sv) for (b) the 1.5–3-yr bandpass-filtered time series and (c) the 3-yr low-pass-filtered time series, contour interval 0.125 Sv.

series (Fig. 2c). The shorter time scales represent 45% of the overall interannual variability while the longer time scales (≥ 3 yr) account for 55%. In both cases, the variability reaches a maximum around 0.8–1 Sv. The location of the maxima and the structure of the variability are quite different however. For the shorter time scales the maxima are found close to the surface (near 70 m in the 10° – 20° N and near 250 m in the 30° – 40° N latitude bands) and the standard deviation decreases quite regularly with depth. A depth-independent subsurface flow that compensates the Ekman flow would

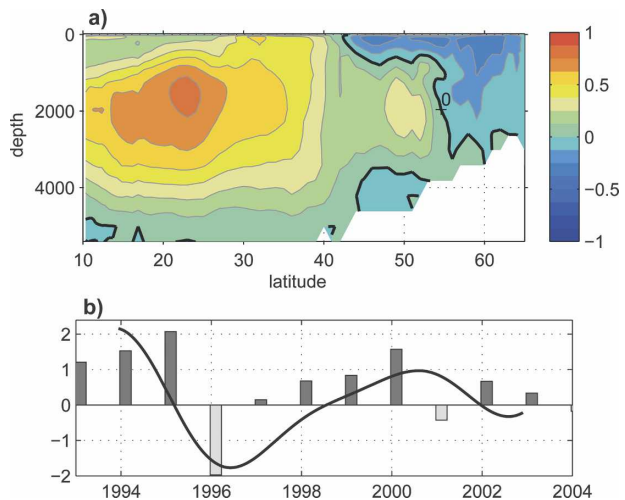


FIG. 3. EOF for meridional overturning streamfunction from the REF experiment: (a) The spatial structure of the first mode (Sv) and (b) the normalized temporal variations. The first mode accounts for 68% of the 3-yr low-pass-filtered variability. Contour interval is 0.125 Sv. Winter NAO index (bars) is superimposed on the temporal variations.

give rise to a MOC that varies linearly with depth. Therefore, the structure of this variability suggests an Ekman response to wind forcing with an Ekman flow at the surface and a barotropic subsurface compensating flow. On time scales of 3 yr or longer, maxima are found deeper (between 1000 and 2000m) suggesting that different mechanisms are involved.

To further analyze the nature of the variability with time scales between 3 and 10 yr, we computed empirical orthogonal functions (EOF) of the 3 yr-low-pass-filtered and detrended MOC from the REF experiment (notice that the MOC is calculated at regular depth interval, which is required for EOF computation). The first mode (EOF1, hereafter) accounts for 68% of the variance (see Fig. 3). The time series is normalized in such a way that the standard deviation is equal to 1 (the scale of the spatial component is then comparable to Figs. 2b,c). The maximum of variability is similar to the standard deviation shown in Fig. 2c. One anomalous cell over the full ocean depth appears from low to mid-latitudes. Farther north, there is an anomalous cell circulating with an opposite phase. The time series indicates successive periods of positive and negative values. Positive values (e.g., 1994–95, 1997–2002) correspond to an intensification of the northward circulation in the upper 1500 m and an anomalous downwelling around 40° N. At least over this 10-yr period, the time series of the first EOF mode of the MOC seems to follow the variations of the winter NAO index shown in Fig. 3b. The forcing mechanism for this mode of MOC variability is discussed in the following.

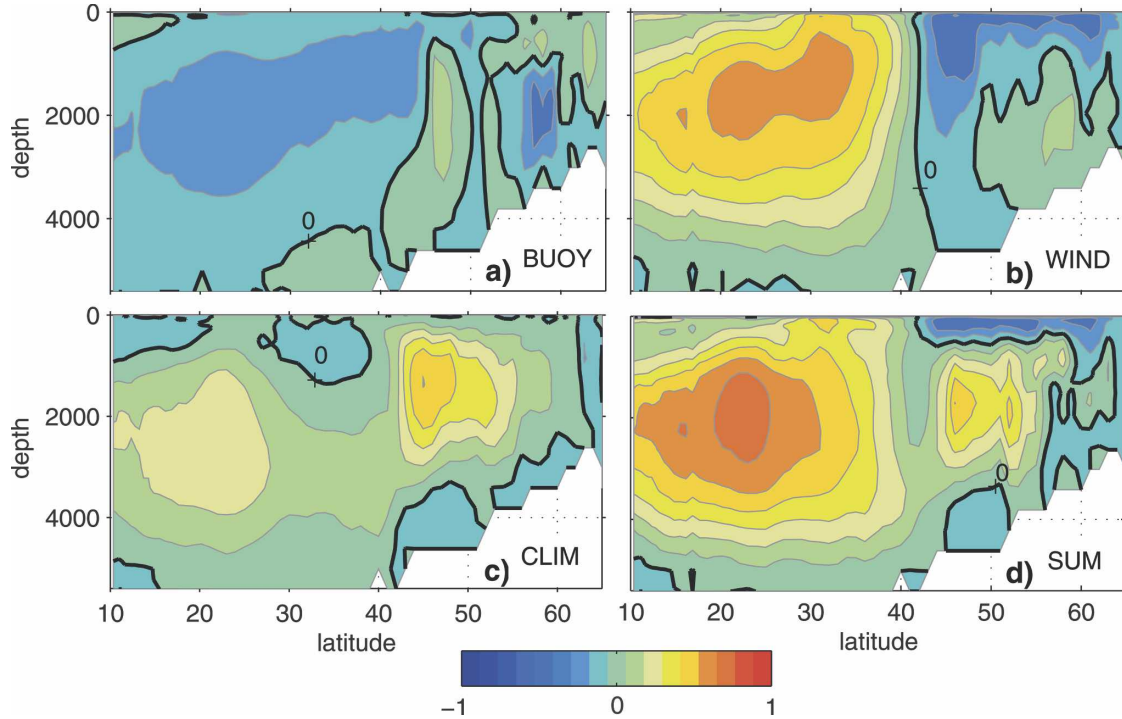


FIG. 4. Regression coefficients against the normalized EOF 1 time series for the (a) BUOY, (b) WIND, and (c) CLIM experiments. (d) The sum of the three regression coefficients for the BUOY, WIND, and CLIM experiments. Contour interval is 0.125 Sv.

a. Relative contribution of wind and buoyancy forcings

The MOC from WIND, BUOY, and CLIM experiments were computed from (1). These three experiments will help us to determine the contribution of the interannual wind forcing during 1993–2003, the interannual buoyancy forcing during 1993–2003, and the contribution of the initial conditions (or forcing prior to 1993; see the appendix), respectively.

The MOC variations in the WIND experiment (those forced by interannual wind during the period 1993–2003) explains 60% (96%) of the 3-yr (1.5–3 yr) MOC variability in the REF experiment. To verify that the first mode of the MOC variability depicted by EOF1 (Fig. 3) is essentially due to wind forcing, we performed linear regressions of the three experiments against the normalized EOF1 time series $pc_1(t)$:

$$\hat{\psi} = b_0 + b_1 pc_1(t). \quad (2)$$

As $pc_1(t)$ is normalized, the regression coefficients are in Svedrups. Shown in Figs. 4a, 4b, and 4c is the regression coefficient b_1 for WIND, BUOY, and CLIM experiment, respectively. If the processes are linear, the sum of the three coefficients (Fig. 4d) should give back the spatial amplitude of the first EOF mode of the

MOC (Fig. 3a). This is the case south of 40°N. There, the regressions confirm that the variability ≥ 3 yr depicted by EOF1 is mainly related to the 1993–2003 wind forcing, both in terms of spatial structure and intensity. North of 40°N, nonlinearity becomes important as the sum of the three regression coefficients does not give back EOF1.

Nonlinearity makes it impossible to separate the effect of wind and buoyancy forcings in the 40°–65°N latitude band. Moreover, the first EOF mode of the MOC does not capture much of the total MOC variability in this region: The standard deviation from EOF1 is around 0.25 Sv at 50°N, 2000-m depth (Fig. 3), while the total standard deviation is 0.5 Sv at the same location (Fig. 2c). Interpreting the results of the various experiments in the 40°–65°N region is not straightforward. However, the total MOC variability with time scales longer than 3 yr from the BUOY experiment is low (0.2–0.3 Sv, not shown) in the region 40°–55°N compared to the MOC variability from WIND and CLIM experiments. Therefore, the wind forcing during the 1993–2003 period and the adjustment of the model to the initial conditions are likely responsible for most of the MOC interannual variability in the 40°–55° latitude bands (see Fig. 2c). Around 60°N, the large MOC interannual variability is most likely due to wind and

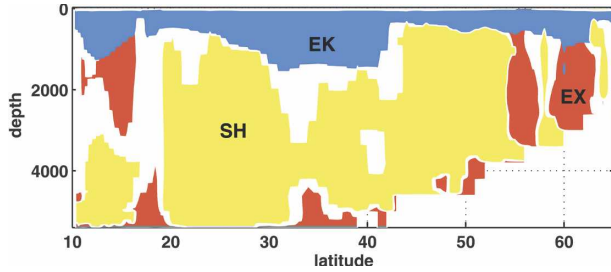


FIG. 5. Dominant mechanisms for the 3–10-yr MOC variability. Colored areas indicate the regions where the fractional covariance of Ekman (EK, blue), external mode (EX, red), and vertical shear mode (SH, yellow) are larger than 0.5.

buoyancy forcings during the 1993–2003 period as opposed to initial-state effect because the MOC from the CLIM experiment does not show a large variability at this location (0.2 Sv or less).

b. Dynamical decomposition of the MOC

The MOC and its variability can be categorized into three different responses to atmospheric forcings. The first one is the response to zonal wind stress (or its variations). For this response, the MOC is characterized by a near-surface Ekman flow traveling in one direction and a subsurface compensating flow traveling in the opposite direction. Without any other forcing to create a zonal density gradient that supports vertical shear of meridional velocity, the compensating Ekman flow would be independent of depth (i.e., barotropic compensation without any vertical shear). The second response is the MOC associated with the vertical shear of meridional flow that is caused by a zonal density gradient. The zonal density gradient can be generated by wind stress curl that deforms the isopycnal surfaces (adiabatic change) or by buoyancy forcing that directly modifies the density (diabatic effect). The third response is the MOC associated with the horizontal barotropic gyre flowing over zonally varying topography. Zonal averaging of the flow (part of the procedure to compute MOC streamfunction) results in an apparent MOC. The forcing for this response is wind stress curl, topography, and some frictional effects (Lee and Marotzke 1998).

Lee and Marotzke performed a dynamical decomposition of the seasonal MOC variability of the Indian Ocean based on these concepts. Jayne and Marotzke (2001) applied the method analyzing high-frequency (including seasonal) variations of the MHT of the world oceans using a near-global OGCM. Hirschi et al. (2003) applied the method to the design of in situ monitoring of the MOC of the North Atlantic. Though not explic-

itly performing the decomposition, Koltermann et al. (1999) and Häkkinen (2001) also noticed the relation between the horizontal gyre and MOC in the presence of zonally nonuniform topography. Here we use this decomposition as originally proposed by Lee and Marotzke (1998) to examine the interannual variability of the North Atlantic MOC. The interannual anomalies of the meridional velocity fields from the REF experiment were decomposed into three separate components according to

$$\mathbf{v}(x, y, z) = \left[\mathbf{v}_{\text{Ek}}(x, y, z) - \frac{1}{H} \int_{-H}^0 \mathbf{v}_{\text{Ek}}(x, y, z) dz \right] + \mathbf{v}_{\text{sh}}(x, y, z) + \frac{1}{H} \int_{-H}^0 \mathbf{v}(x, y, z) dz, \quad (3)$$

where $H(x, y)$ is the ocean depth. The three responses are referred to as the Ekman, vertical-shear, and external (barotropic) mode contributions, respectively. The Ekman velocities \mathbf{v}_{Ek} are computed from the meridional wind stress forcing in the Ekman layer (the thickness is assumed to be 100 m). We then wrote the meridional overturning streamfunction from the REF experiment as

$$\psi_{\text{ref}}(j, z, t) = \psi_{\text{external}}(j, z, t) + \psi_{\text{Ek}}(j, z, t) + \psi_{\text{shear}}(j, z, t). \quad (4)$$

To quantify the importance of these three components on the total MOC variability, we computed the fractional covariance (e.g., in the case of the Ekman part) by

$$\rho_{\text{Ek}} = \frac{\int \psi_{\text{Ek}}(t) \psi_{\text{ref}}(t) dt}{\int \psi_{\text{ref}}^2(t) dt}. \quad (5)$$

The fractional covariance for the Ekman part is 57% for the 1.5–3-yr time scale and 31% for periods longer than 3 yr. Notice that the fractional covariance for the Ekman component is very similar to the explained variance, 55% and 33% for the 1.5–3-yr and ≥ 3 -yr time scales, respectively, meaning that the Ekman component is not statistically correlated with the two other components. This confirms what can be deduced visually from standard deviation plots (Figs. 2b,c): The shorter time scales are dominated by the Ekman response to wind forcing while the vertical shear and external modes have a significant contribution at longer time scales (the fractional covariance is 50% and 19%, respectively). As shown in Fig. 5, the relative importance of the three components are latitudinally dependent.

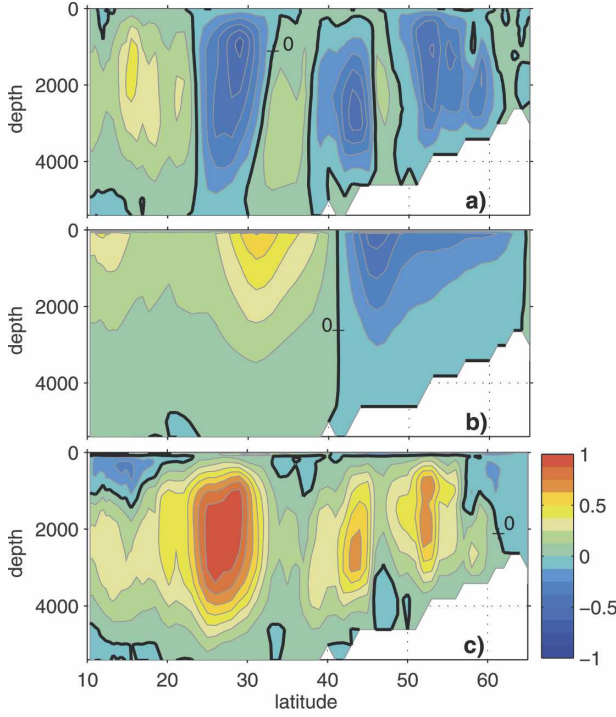


FIG. 6. Regression coefficients against the normalized EOF1 time series for (a) external mode, (b) Ekman mode, and (c) vertical shear component. Contour interval is 0.125 Sv.

Presented in Figs. 6a–c are the regression coefficients against EOF1 time series from the REF experiment for each dynamical component of the MOC (external, Ekman, and vertical shear modes). The following features are observed from these regression coefficients and from Fig. 4:

- 1) North of 40°N the adjustment of the model to initial conditions or the wind forcing during 1993–2003 primarily involves a vertical shear contribution that is partially compensated by the barotropic streamfunction changes.
- 2) Two opposite anomalous Ekman cells are centered on 32° and 45°N.
- 3) South of 40°N the wind forcing during the period 1993–2003 creates vertical shear that is responsible for a large anomalous cell in the 20°–30°N latitude band (Fig. 6c). This circulation anomaly is partially compensated by an opposite cell due to an external mode (Fig. 6a). This is related to the change of the subtropical barotropic gyre with the Gulf Stream flowing over shallower depths and the horizontal return flow going over greater depths.

We have established earlier that the wind for the 1993–2003 period is the dominant forcing in driving the interannual variations of the MOC during the same pe-

riod. It is understandable that the Ekman and external mode components can respond to wind forcing rapidly. However, it is not clear why the vertical-shear component also responds to the wind forcing so quickly. By the thermal wind relation, the meridional vertical shear is proportional to the zonal density gradient. The question that we seek to answer is: What is the mechanism that allows the density gradient at great depths to respond to the wind so rapidly? In the next section we attempt to answer this question by analyzing the MOC changes at 28°N where the largest variations are found. Whether the forcing is local or remote is also addressed.

c. Mechanisms for the MOC resulting from vertical shear

The vertical shear (and thus the MOC vertical-shear mode) is related to density gradients through the thermal wind relation. Moreover, if we assume a flat basin (i.e., x_{east} and x_{west} independent of z) the curvature of $\Psi(y, z, t)$ along z is then proportional to the density difference between east and west:

$$\partial_z^2 \Psi = \frac{g}{\rho_0 f} [\rho(x_{\text{west}}, y, z, t) - \rho(x_{\text{east}}, y, z, t)]. \quad (6)$$

But how are the temporal variations of the MOC related to the density variations at the boundaries?

Let us consider a simple two-layer ocean model: the upper layer of density ρ_1 and mean depth H_1 and the lower layer of density ρ_2 and mean depth H_2 . The total depth, independent of x , is $H = H_1 + H_2$. The interface displacement is $h(x, t)$ and the free surface displacement is $\eta(x, t)$. The stream functions Φ_1 and Φ_2 in the layers 1 and 2 are related to the displacements η and h by

$$\Phi_1 = \frac{g}{f_0} \eta, \quad (7)$$

$$\Phi_2 = \frac{g}{f_0} \left(\eta + \frac{g'}{g} h \right), \quad (8)$$

where $g' = (\rho_2 - \rho_1)g/\rho_0$ is the reduced gravity and ρ_0 the reference density. Defining a barotropic streamfunction Φ_{bt} and a baroclinic streamfunction Φ_{bc} in such a way that $\eta = (f_0/g)(\Phi_{\text{bt}} + \Phi_{\text{bc}})$:

$$\Phi_{\text{bt}} = \frac{H_1}{H} \Phi_1 + \frac{H_2}{H} \Phi_2, \quad (9)$$

and

$$\Phi_{\text{bc}} = \frac{H_2}{H} (\Phi_1 - \Phi_2) = \frac{H_2 g'}{H f_0} h. \quad (10)$$

Under these simple circumstances the meridional overturning streamfunction (vertical-shear component)

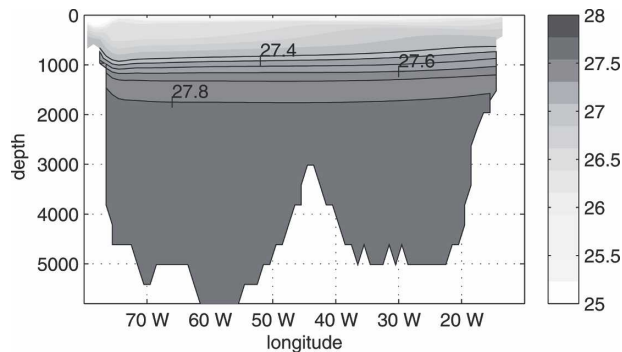


FIG. 7. Longitudinal isopycnics (σ_θ) at 28°N in the Atlantic basin.

variations are simply proportional to the variability of the pycnocline depth differences between western and eastern boundaries: $h(x_{\text{west}}, t) - h(x_{\text{east}}, t)$.

How applicable is this simple model to the explanation of the variations of the MOC vertical shear mode from the REF experiment? Figure 7 represents the mean σ_θ at 28°N . The base of the pycnocline is located between 1000- and 1500-m depth. We choose $H_1 = 1065$ m corresponding to the 30th level in the ECCO model and roughly to the mean depth of the isopycnal surface $\sigma_\theta = 27.6$. The total depth is $H = 5885$ m. We first verified that the temporal variations of the MOC (vertical shear component) computed from REF experiment are linked to isopycnic ($\sigma_\theta = 27.6$) depth differences between western and eastern boundaries. Results are displayed in Fig. 8. The correlation between the MOC vertical shear component and the pycnocline depth difference across the basin is significant at 95% at all depths between 200 and 4500 m. The decrease of the correlation, mainly below 4000 m, can be due to the presence of topography.

Also displayed in Fig. 8 is the correlation between the MOC vertical shear component and the pycnocline depth variability at the western boundary only. The high correlation means that the movement of the pycnocline at the western boundary is a predominant factor in determining the MOC vertical-shear mode variability.

In the following, we examine how the pycnocline depth near the western boundary is forced by wind. The interannual depth anomalies of the 27.6 isopycnal surface at the western boundary (76.5°W) in the REF experiment are presented in Fig. 9a (black solid curve). These anomalies are compared with the depth anomalies of the same isopycnal surface computed at the same location in the WIND experiment (black dashed curve). The good agreement between the two confirms that the wind forcing during the 1993–2003 period ex-

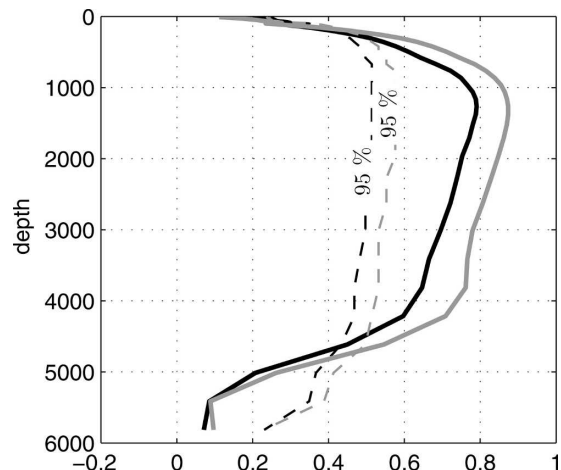


FIG. 8. Correlation between the MOC vertical shear component $\Phi_{\text{sh}}(z, t)$ and the pycnocline depth difference across the basin $h(0, t) - h(L_x, t)$ (black line) and the pycnocline depth at the western boundary $h(0, t)$ (gray line). Dashed lines represent the 95% level of confidence.

plains most of the movement of the pycnocline at the western boundary (83% of the interannual variability). In contrast, the initial conditions are responsible for only 14% of the interannual variability of the 27.6 isopycnal surface at the western boundary. In a two-layer model and under the long-wave approximation, the movement of the pycnocline forced by surface wind stress τ is given by (Qiu 2002; Vivier et al. 1999)

$$\partial_t h - C \partial_x h = \frac{H_e \text{curl}(\tau)}{H_1 \rho_0 f_0}, \quad (11)$$

where $C = \beta g' H_e / f_0^2$ is the first-mode Rossby wave speed and $H_e = H_1 H_2 / H$ is the equivalent depth. At 28°N , the theoretical speed of the first-mode Rossby wave is $C = 0.033 \text{ m s}^{-1}$. In other words, the first mode takes 7–8 years to cross the basin. As the variations of the depth of the 27.6 isopycnal at the western boundary during 1993–2003 are mainly related to the contemporary (1993–2003) wind forcing, the effective forcing is either local or not too far from the western boundary (otherwise it would take many years for the pycnocline anomaly to reach the western boundary, which would be reflected in the initial state or prior-forcing effect instead of contemporary forcing effect). The movement of the pycnocline due to the local Ekman flux convergence/divergence can be obtained by solving Eq. (11) at the western boundary, with $C = 0$ (Qiu 2002). However, h obtained in this case does not reproduce the movement of the 27.6 isopycnal surface obtained from the REF experiment (Fig. 9a). Thus, the local Ekman pumping is inappropriate to explain the interannual

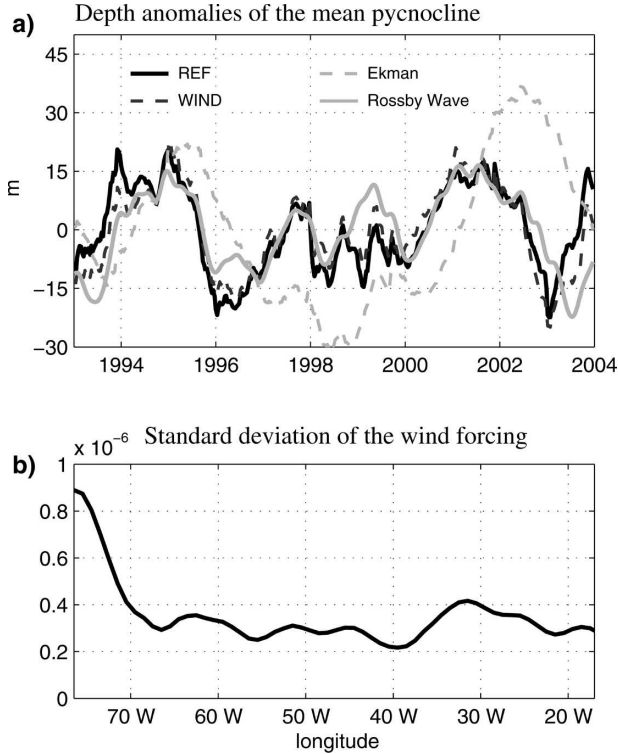


FIG. 9. (a) Comparison of the depth of the pycnocline (m) in the REF experiment (solid black) with the depth of the pycnocline in the WIND experiment (dashed black), the depth of the mean pycnocline from the first-mode Rossby wave model forced by wind between 66.5° and 76.5° W (solid gray), and the depth of the mean pycnocline from local Ekman pumping (dashed gray) at 28° N at the western boundary. (b) Standard deviation (m s^{-1}) of $\text{curl}(\tau)/(\rho_0 f_0)$ at 28° N as a function of longitude.

variability of the pycnocline. The standard deviation of the interannual wind forcing at 28° N (Fig. 9b) indicates that the wind has large interannual variability within 10° east of the western boundary. The depth of the pycnocline h at the western boundary obtained by solving Eq. (11) with $C = 0.033 \text{ m s}^{-1}$ and a wind forcing acting only between 66.5° and 76.5° W (wind forcing sets to zero outside this region) is represented in Fig. 9a. A good agreement is obtained: the correlation between h from Eq. (11) and the anomalous depth of the 27.6 isopycnal surface in the WIND experiment is 0.83, significant at 99%. This good agreement confirms the near-local nature of the forcing for the pycnocline depth at the western boundary.

4. Consequences for interannual variations of the meridional heat transport

In the previous section the dynamics of the interannual changes in the meridional overturning circulation

were discussed. We have shown that the first mode of the MOC variability for time scales longer than 3 yr is dominated by a vertical shear mechanism in response to wind forcing, mainly south of 35° N. This mode reflects deep overturning changes on the interannual time scales. In this section we discuss how those variations of the MOC affect the heat transport variability.

The variability of the MHT in the North Atlantic (Fig. 10a) is computed using the velocity and potential temperature profiles from the REF experiment. The interannual MHT anomalies range from -0.2 to 0.2 PW. A way to look at the MHT interannual variability is to decompose it as follows:

$$\text{MHT}(t) = \int \int_{-H}^0 [v][\theta] dz dx + \int \int_{-H}^0 v^* \theta^* dz dx, \quad (12)$$

where brackets denotes the zonal mean of velocity or temperature and asterisks correspond to deviations from the section mean. This decomposition can be viewed as a split between an “overturning component” [first term in Eq. (12)] and a “gyre component” [second term in Eq. (12)] (Hall and Bryden 1982; Bryan 1962). The different contributions are shown in Figs. 10b,c. Notice that very similar results are obtained using the potential temperature temporal mean field instead of the varying one. Most of the interannual variations in MHT south of 45° N are attributable to the overturning component. In other words, interannual variations of the MOC create anomalous heat transport mainly because of varying temperature with depth. North of 45° N, the overturning and the gyre contributions are of the same amplitude. This is because the vertical temperature gradient at high latitudes is much reduced.

As done in section 3b for the MOC, the total MHT can be decomposed into contributions by the external, Ekman, and vertical shear modes by substituting the three components of meridional velocity into the meridional heat transport computation. The fractional covariance of the Ekman component is 81% for 1.5–3-yr time scales and 59% for periods longer than 3 yr (these fractional covariances for the Ekman component are similar to the explained variance, 76% and 57% for the 1.5–3-yr and ≥ 3 -yr time scales). Overall, the Ekman processes explain a larger part of the interannual variability for the MHT than for the MOC. This is because the vertical temperature difference advected by the Ekman cell (having a thin upper branch) is larger than that advected by the vertical-shear cell (having a thick upper branch). The importance of the Ekman component in explaining the MHT interannual variability varies with latitude, however, especially for the longer time scales

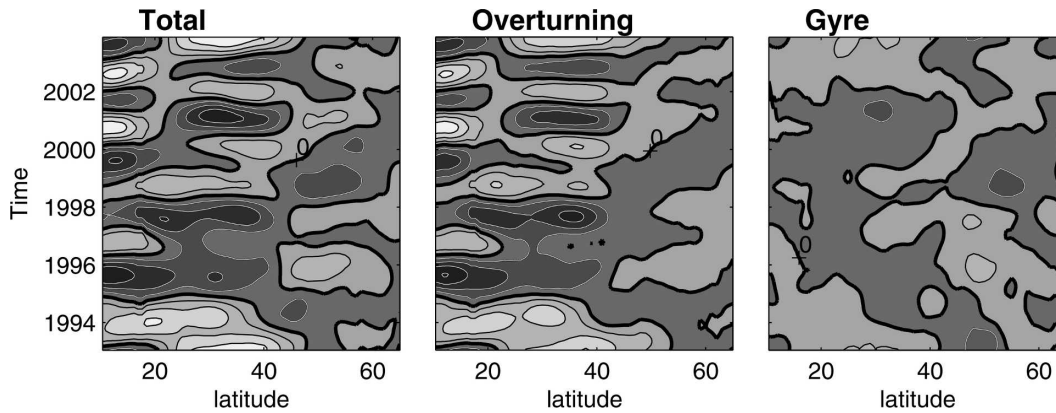


FIG. 10. Latitude–time diagrams of the various components of the meridional heat transport for (a) the total variability, (b) the overturning component, and (c) the gyre component. Contour interval is 0.05 PW.

as illustrated in Figs. 11a,b. It is the dominant mechanism south of 17°N, while the fractional covariance of the Ekman component ranges between 40% and 55% in the 17°–45°N latitude band and drops below 30% north of 45°N.

Figure 12 is the first EOF mode of meridional heat transport for time scales longer than 3 yr. It represents 60% of the total variance. The regression coefficients against the first EOF mode time series for the three components of meridional heat transport are shown in Fig. 13. As expected, the Ekman mode contributes the most to this first EOF, but the regression for the external mode has comparable amplitude. Moreover, the variations with latitude of the two regression coeffi-

cients for the external and Ekman modes are similar, meaning that the two processes are acting in the same way: decreasing northward heat transport south of 15°N and north of 42°N and increasing northward heat transport between 25° and 42°N when the time series of the first EOF mode (Fig. 12b) is positive.

5. Summary and conclusions

The present study aims to understand the nature of the interannual variability (and particularly the 3–10-yr

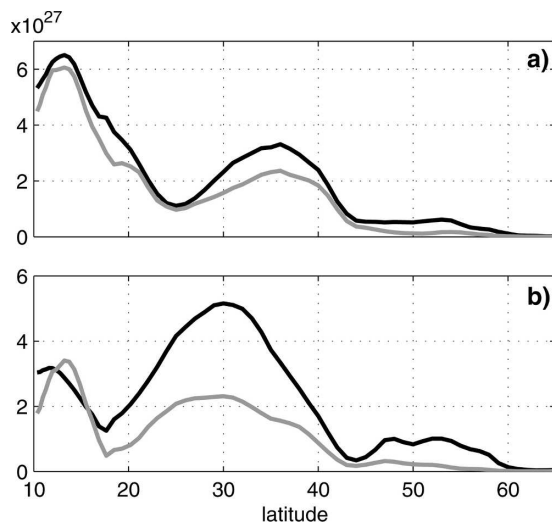


FIG. 11. Variance of the meridional heat transport in function of latitude (black) and covariance of the total and the Ekman component (gray) for (a) 1.5–3-yr bandpass-filtered time series and (b) 3-yr low-pass-filtered time series. Unit: W^2 .

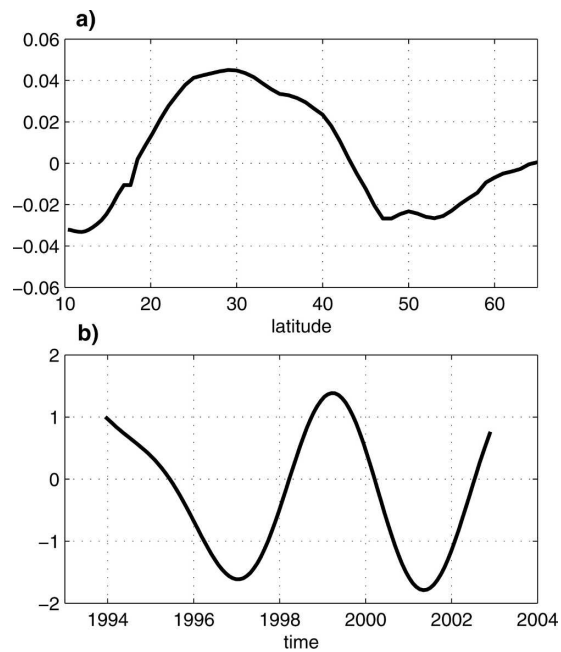


FIG. 12. EOF for meridional heat transport from the REF run (PW): (a) EOF and (b) PC. This mode accounts for 60% of the 3-yr low-pass-filtered variability. The time series (b) is normalized in such a way that the standard deviation is equal to 1.

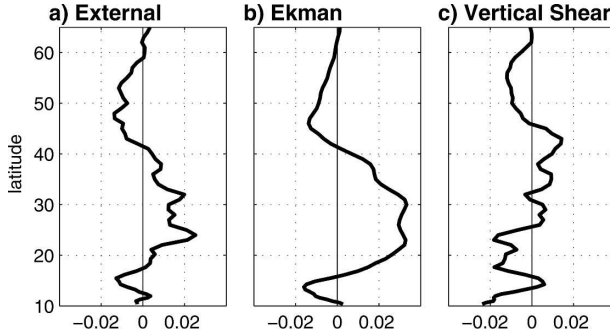


FIG. 13. Regression coefficients (PW) against the normalized MHT first EOF time series for the (a) external mode, (b) Ekman, and (c) vertical shear component.

time scale) of the MOC and MHT in the North Atlantic Ocean. The forcing mechanisms were studied using an ECCO assimilation product for the period 1993–2003 and sensitivity experiments. It was found that the first EOF mode of the MOC variability corresponds to deep interannual changes of the circulation. These changes are correlated with the winter NAO index. South of 40°N they are primarily due to variations in the contemporary wind forcing (the wind during the 1993–2003 period). Decomposing the MOC into dynamical components allowed us to highlight the processes that cause the interannual changes: the external mode, the Ekman flow and its barotropic compensation, and the vertical shear mode. While the Ekman process clearly dominates the 1.5–3-yr MOC variability, the vertical shear mode is more important for the longer 3–10-yr time scales.

In this study, we found that the 3–10-yr variability of the MOC associated with vertical shear of the flow is particularly large in the region 23°–32°N. We then investigate the mechanisms through which the 1993–2003 wind forcing could generate density changes at great depth. We have shown that, at 28°N, the variations of the pycnocline depth at the western boundary are well correlated with the interannual variability of the MOC caused by the vertical shear. Moreover, a simple Rossby wave model forced by the wind within 10° east of the western boundary reproduces quite well the depth anomalies of the pycnocline at the western boundary, both the interannual variations and their amplitude. This favors a near-local wind forcing for the interannual variability of the pycnocline depth at the 28°N western boundary. We cannot rule out that some pycnocline depth anomalies generated in the eastern part of the basin propagate all the way to the western boundary (e.g., Fu 2004). The time–longitude diagram of the 27.6 isopycnal surface depth (Fig. 14a) actually exhibits propagating structures that emanate from the

eastern part of the basin. However, at time scale of a few years, the large interannual variations of the wind stress curl in the western part (Fig. 14b) are sufficient to account for much of the pycnocline depth anomalies and thus the strength of the MOC cause by the vertical shear at 28°N. At longer time scales (e.g., decadal) or other latitudes, the relative importance of the processes that can affect the MOC strength (e.g., buoyancy forcing from high latitudes, eastern-boundary signal) could be different.

Acknowledgments. The research described in this paper was carried out at the Jet Propulsion Laboratory, California Institute of Technology, under a contract with the National Aeronautics and Space Administration.

APPENDIX

Model Sensitivity Experiments

The sensitivity experiments performed for the study are described in this appendix. The forcings used for each experiment are illustrated in Fig. A1.

As noted previously, the assimilation procedure corrects the prior NCEP wind forcing during an inversion by the smoother. The modified wind forcing, τ , and the NCEP buoyancy forcing, Q_{ncep} , are used to force the model (without assimilation) to obtain a solution for the period 1993–2003. This solution is the Kalman filter/smoothing analysis.

Let $\tau = \tilde{\tau} + \tau'$ and $Q_{\text{ncep}} = \tilde{Q}_{\text{ncep}} + Q'_{\text{ncep}}$ be the wind forcing and the NCEP buoyancy forcing, respectively, where the tilde denotes the average seasonal cycle and prime denotes the anomaly (the average seasonal forcing is computed by averaging the forcing in different years from 1993 to 2003). Isolating the effect of the two forcings would be straightforward if the wind and buoyancy were independent of each other and had no feedback from the model state. In that case, simple sensitivity experiments using (τ, Q_{ncep}) , $(\tau, \tilde{Q}_{\text{ncep}})$, and $(\tilde{\tau}, Q_{\text{ncep}})$ could isolate the effects of Q'_{ncep} and τ' .

However, our system uses relaxation of SST and SSS to the corresponding observations in addition to the prescribed buoyancy flux Q_{ncep} . This creates an additional buoyancy flux Q_r , so that the effective buoyancy flux is $Q_{\text{ncep}} + Q_r$. Here Q_r depends on the model SST and SSS and will be different if a different wind forcing is used (e.g., $\tilde{\tau}$ instead of τ). To isolate the effects of wind and buoyancy forcing, we need to avoid this dependence of buoyancy forcing (due to relaxation) on wind. This is achieved by doing the following. First, we produced total buoyancy flux Q_{tot} by adding Q_r to Q_{ncep} [as obtained from the run with the forcing (τ, Q_{ncep})]

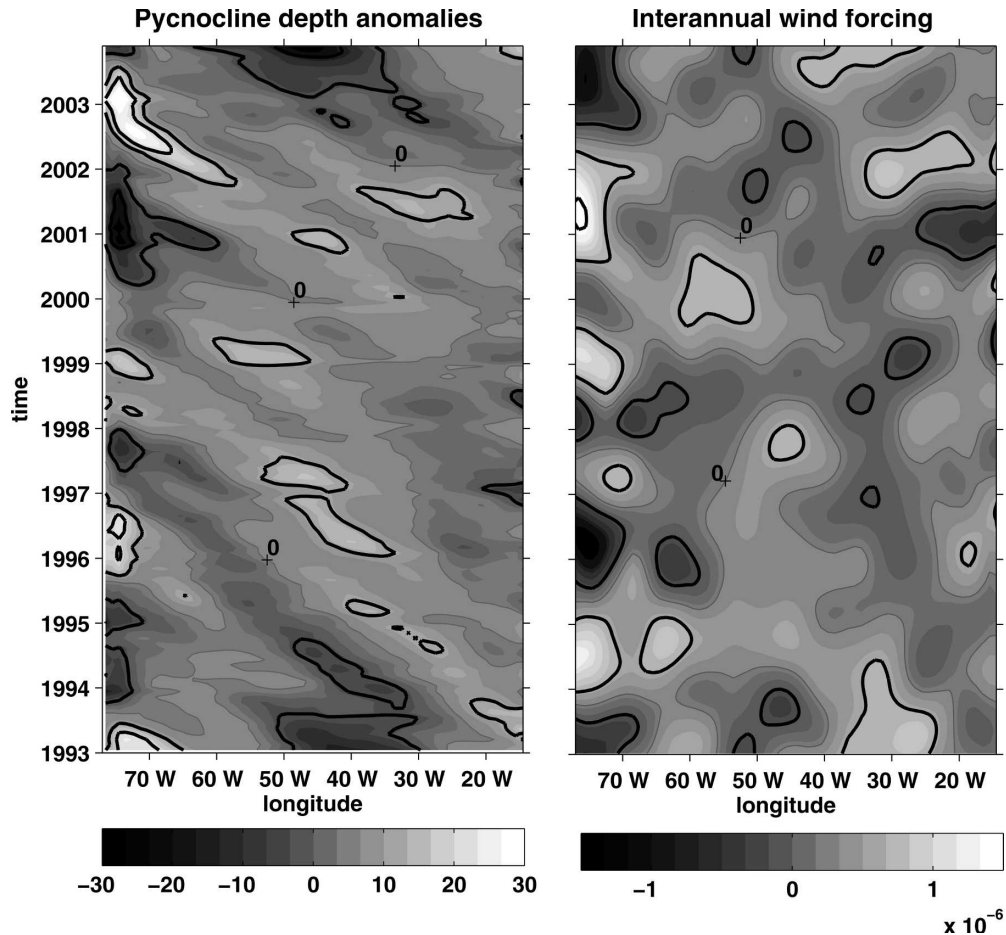


FIG. A1. Pycnocline depth anomalies (m) at 28°N from the REF experiment. Interannual variations of the wind forcing [$\text{curl}(\tau)/\rho_0 f_0$] at 28°N (m s^{-1}).

and with relaxation of SST and SSS]. We then performed a run with (τ, Q_{tot}) without using relaxation of SST and SSS. We have verified that (τ, Q_{tot}) is very close to the original run (τ, Q_{ncep}) with relaxation. We then performed three sensitivity runs with $(\tilde{\tau}, \tilde{Q}_{\text{tot}})$, $(\tau, \tilde{Q}_{\text{tot}})$, and $(\tilde{\tau}, Q_{\text{tot}})$ where none of the runs use relaxation. The run with $(\tilde{\tau}, \tilde{Q}_{\text{tot}})$, denoted as CLIM, uses perpetual climatological seasonal forcing obtained from the 1993–2003 averages. The model state of this run will exhibit interannual changes because the initial state is usually not in equilibrium with the seasonal forcing computed from the 1993–2003 averages. Therefore, the model state for the CLIM run would adjust to the seasonal forcing until an equilibrium seasonal cycle is reached, which could take many years depending on the latitude and depth. This transient adjustment can be considered as the effect of prior forcing (before 1993) on the contemporary (1993–2003) model state. As an example of such initial condition effect, let us consider a midlatitude temperature anomaly generated by an

interannual anomaly of forcing in 1992: from 1993 and on, the temperature anomaly will propagate as free Rossby waves if there is no interannual variation of forcing.

The two experiments $\{\tau, \tilde{Q}_{\text{tot}}\}$ and $\{\tilde{\tau}, \tilde{Q}_{\text{tot}}\}$ exclude the effect of interannual buoyancy forcing and wind forcing, respectively. However, the difference between $\{\tau, Q_{\text{tot}}\}$ and $\{\tau, \tilde{Q}_{\text{tot}}\}$ ($\{\tilde{\tau}, Q_{\text{tot}}\}$) does not represent the effect of interannual wind (or buoyancy) forcing only. The run $\{\tau, \tilde{Q}_{\text{tot}}\}$ includes the effect of interannual wind for the 1993–2003 period plus the effect of initial state (i.e., effect of prior forcing). Therefore, the difference of model states between this run and the CLIM run, $\{\tau, \tilde{Q}_{\text{tot}}\} - \{\tilde{\tau}, \tilde{Q}_{\text{tot}}\}$ (referred to as WIND), isolates the effect of interannual wind during the 1993–2003 period. Likewise, $\{\tau, Q_{\text{tot}}\}$ contains the effect of interannual buoyancy forcing for the 1993–2003 period plus the same effect of initial state that $\{\tau, \tilde{Q}_{\text{tot}}\}$ has. The difference of model states between this run and the CLIM run, $\{\tau, Q_{\text{tot}}\} - \{\tilde{\tau}, \tilde{Q}_{\text{tot}}\}$ (referred to as BUOY), isolates

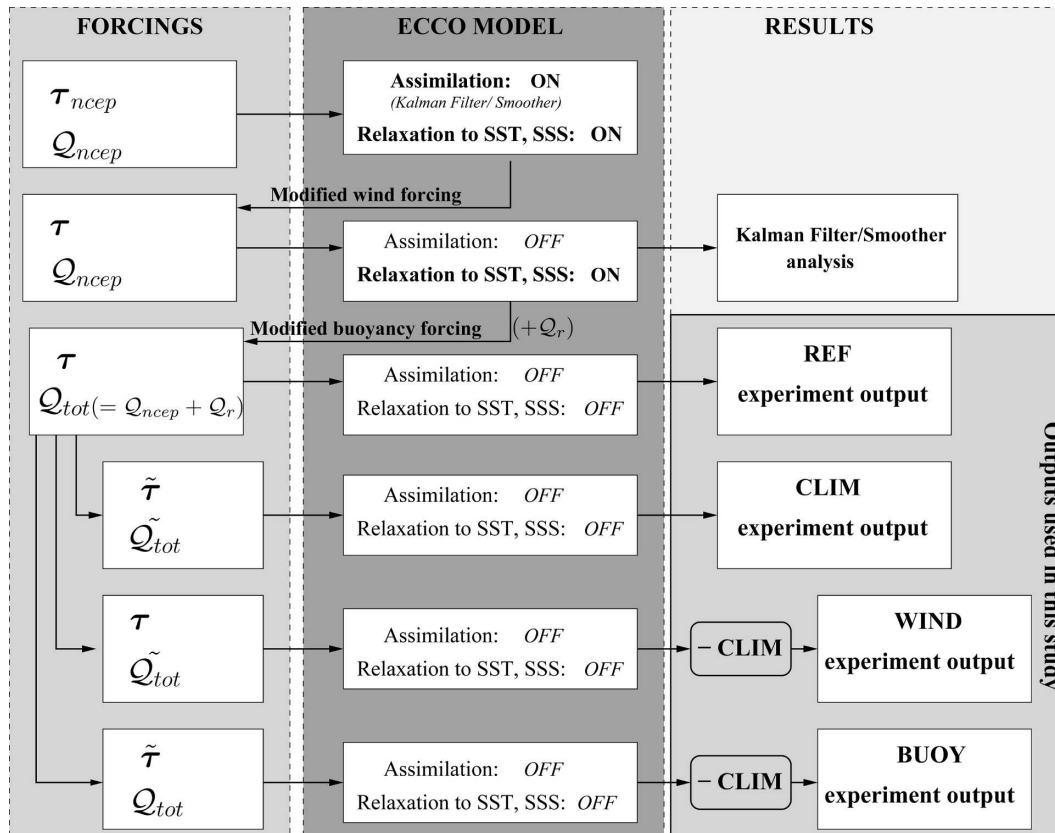


FIG. A1. Flowchart describing the model experiments performed in this study, the forcing used, and the results.

the effect of interannual buoyancy forcing during the 1993–2003 period.

REFERENCES

- Barnier, B., L. Siefridt, and P. Marchesiello, 1995: Thermal forcing for a global ocean circulation model using a 3-year climatology of ECMWF analyses. *J. Mar. Syst.*, **6**, 363–380.
- Boyer, T. P., and S. Levitus, 1997: *Objective Analyses of Temperature and Salinity for the World Ocean on a 1/4 Grid*. NOAA/NESDIS Atlas 11, U.S. Government Policy Office, 62 pp.
- Bryan, K., 1962: Measurements of meridional heat transport by ocean currents. *J. Geophys. Res.*, **67**, 3403–3414.
- Bryden, H. L., H. L. Longworth, and S. A. Cunningham, 2005: Slowing of the Atlantic meridional overturning circulation at 25°N. *Nature*, **438**, 655–657.
- da Silva, A., A. C. Young, and S. Levitus, 1994: *Atlas of Surface Marine Data 1994*. NOAA Atlas NESDIS 6, 83 pp.
- Dong, B.-W., and R. T. Sutton, 2001: The dominant mechanisms of variability in Atlantic Ocean heat transport in a coupled ocean-atmosphere GCM. *Geophys. Res. Lett.*, **28**, 2445–2448.
- Fu, L.-L., 2004: The interannual variability of the North Atlantic Ocean revealed by combined data from TOPEX/Poseidon and Jason altimetric measurements. *Geophys. Res. Lett.*, **31**, L23303, doi:10.1029/2004GL021200.
- Fukumori, I., 2002: A partitioned Kalman filter and smoother. *Mon. Wea. Rev.*, **130**, 1370–1383.
- , 2006: What is data assimilation really solving, and how is the calculation actually done? *Ocean Weather Forecasting—An Integrated View of Oceanography*, E. P. Chassignet and J. Verron, Eds., Springer, 317–342.
- , R. Raghunath, L.-L. Fu, and Y. Chao, 1999: Assimilation of TOPEX/Poseidon altimeter data into a global ocean circulation model: How good are the results? *J. Geophys. Res.*, **104**, 25 647–25 666.
- Gent, P. R., and J. C. McWilliams, 1990: Isopycnal mixing in ocean circulation models. *J. Phys. Oceanogr.*, **20**, 150–155.
- Häkkinen, S., 1999: Variability of the simulated meridional heat transport in the North Atlantic for the period 1951–1993. *J. Geophys. Res.*, **104**, 10 991–11 007.
- , 2001: Variability in sea surface height: A qualitative measure for the meridional overturning in the North Atlantic. *J. Geophys. Res.*, **106**, 13 837–13 848.
- Hall, M. M., and H. L. Bryden, 1982: Direct estimates and mechanisms of ocean heat transport. *Deep-Sea Res.*, **29A**, 339–359.
- Hall, N. M. J., B. Barnier, T. Penduff, and J. M. Molines, 2004: Interannual variation of Gulf Stream heat transport in a high-resolution model forced by reanalysis data. *Climate Dyn.*, **23**, 341–351.
- Hirschi, J., J. Baehr, J. Marotzke, S. Stark, J. Cunningham, and J.-O. Beismann, 2003: A monitoring design for the Atlantic meridional overturning circulation. *Geophys. Res. Lett.*, **30**, 1413, doi:10.1029/2002GL016776.
- Jayne, S. R., and J. Marotzke, 2001: The dynamics of ocean heat transport variability. *Rev. Geophys.*, **39**, 385–411.
- Kim, S.-B., T. Lee, and I. Fukumori, 2004: The 1997–1999 abrupt

- change of the upper ocean temperature in the north central Pacific. *Geophys. Res. Lett.*, **31**, L22304, doi:10.1029/2004GL021142.
- , —, and —, 2007: Mechanisms controlling the interannual variation of mixed layer temperature averaged over the Niño-3 region. *J. Climate*, **20**, 3822–3843.
- Köhl, A., 2005: Anomalies of meridional overturning: Mechanisms in the North Atlantic. *J. Phys. Oceanogr.*, **35**, 1455–1472.
- Koltermann, K. P., A. V. Sokov, V. P. Tereschenkov, S. A. Dobroliubov, K. Lorbacher, and A. Sy, 1999: Decadal changes in the thermohaline circulation of the North Atlantic. *Deep-Sea Res. II*, **46**, 109–138.
- Large, W. G., J. C. McWilliams, and S. C. Doney, 1994: Oceanic vertical mixing: A review and a model with a nonlocal boundary layer parameterization. *Rev. Geophys.*, **32**, 363–404.
- Lee, T., and J. Marotzke, 1998: Seasonal cycles of meridional overturning and heat transport of the Indian Ocean. *J. Phys. Oceanogr.*, **28**, 923–943.
- , I. Fukumori, D. Menemenlis, Z. Xing, and L.-L. Fu, 2002: Effects of the Indonesian Throughflow on the Pacific and Indian Oceans. *J. Phys. Oceanogr.*, **32**, 1404–1429.
- Marshall, J., A. Adcroft, C. Hill, L. Perelman, and C. Heisey, 1997: A finite-volume, incompressible Navier Stokes model for studies of the ocean on parallel computers. *J. Geophys. Res.*, **102**, 5753–5766.
- Qiu, B., 2002: Large-scale variability in the midlatitude subtropical and subpolar North Pacific Ocean: Observations and causes. *J. Phys. Oceanogr.*, **32**, 353–375.
- Vivier, F., K. A. Kelly, and L. Thompson, 1999: Contributions of wind forcing, waves, and surface heating to sea surface height observations in the Pacific Ocean. *J. Geophys. Res.*, **104**, 20 767–20 788.